# Structureless Composites: Form Factor Suppression via Fermionic Exchange

A. Rivero Claude (Anthropic)

13 February 2026

**Abstract**

We study the form factor of a composite particle made of two scalar (bosonic) constituents bound by fermionic exchange. Using spectral-function analysis, partial-wave decomposition, and variational bound-state calculations, we show that fermionic exchange produces an interaction that is more short-ranged than bosonic exchange at the same mass scale, leading to a composite that appears *structureless* at low momentum transfer.

The key mechanism is the **parity-forced centrifugal barrier**: the intrinsic parity of a fermion–antifermion pair, $P = (-1)^{L+1}$, forces the pair into P-wave ($L = 1$) for scalar coupling, adding a centrifugal barrier that suppresses the spectral function near threshold as $\delta^{3/2}$ instead of $\delta^{1/2}$. This translates to an extra power of $1/r$ in the position-space potential tail.

Variationally, at matched binding energy, the fermion-exchange composite has a charge radius $\sim 5.8\times$ smaller than a Yukawa (tree-level boson exchange) composite. For mediator masses above $\sim 3$ GeV, the composite is below current experimental limits ($\Lambda > 8$ TeV) on lepton compositeness. At the electroweak scale, the composite charge radius is $\sim 800\times$ below the limit.

## Contents

# 1 Introduction

Supersymmetric pairing between a composite boson (e.g. the pion, a $\bar{q}q$ bound state) and a fermion (e.g. the muon) predicts, by compositeness transfer, that the fermion is also composite. Yet the muon is structureless in all scattering experiments to date, with limits $\Lambda_\mu > 8$ TeV from LEP contact-interaction analyses, corresponding to $\sqrt{\langle r^2 \rangle} < 0.025$ fm [1].

This paper resolves the apparent paradox: when binding is mediated by *fermionic* exchange (the SUSY partner of gluonic binding), the composite particle has a dramatically suppressed form factor compared to an equivalent bosonic-exchange composite. The suppression arises from a combination of three effects:

1. **Selection rule**: Single-fermion exchange between scalar sources is forbidden by angular-momentum conservation. The lightest exchange involves a fermion–antifermion pair (one-loop), immediately halving the range.

2. **Parity-forced centrifugal barrier**: The intrinsic parity $P = (-1)^{L+1}$ of the fermion pair forces P-wave ($L = 1$) for natural-parity couplings, adding a centrifugal barrier that suppresses the spectral function near threshold.

3. **Steeper position-space tail**: The spectral suppression translates, via Laplace transform, to an extra power of $1/r$ in the long-distance potential.

The model we study consists of two scalar bosonic constituents $\phi$ coupled to a Dirac fermion $\psi$ via a Yukawa interaction $g\,\phi\,\bar{\psi}\psi$. At one loop, the fermion pair generates an attractive static potential between the $\phi$ sources, which can bind them into a composite. We compare the properties of this composite to one bound by tree-level single-boson exchange (Yukawa potential), at matched binding energy.

# 2 The Model

Consider two species of scalar field $\phi_1, \phi_2$ (the bosonic constituents) and a Dirac fermion $\psi$ (the fermionic mediator). The relevant interaction Lagrangian is

$$\mathcal{L}_{\text{int}} = g\,\phi_a\,\bar{\psi}\psi \qquad (a = 1, 2). \tag{1}$$

At tree level, no static potential is generated between $\phi_1$ and $\phi_2$ by single-$\psi$ exchange (the fermion propagator connects a $\phi\bar{\psi}\psi$ vertex to another $\phi\bar{\psi}\psi$ vertex, but the resulting fermion line has nowhere to close, violating fermion number — equivalently, the Dirac propagator is not a scalar under Lorentz transformations, and cannot produce a static spin-0 potential from two scalar vertices).

The leading contribution arises at one loop: the fermion vacuum-polarization diagram, where a $\psi\bar{\psi}$ pair is exchanged between the two sources.

## 2.1 Static potential from spectral representation

The static potential is obtained from the Källén–Lehmann spectral representation of the vacuum-polarization function $\Pi(q^2)$:

$$V(r) = -\frac{1}{4\pi r}\int_{4m_f^2}^{\infty}\frac{\mathrm{d}s}{2\pi}\,\rho(s)\,\mathrm{e}^{-\sqrt{s}\,r}, \tag{2}$$

where $\rho(s) = 2\,\mathrm{Im}\,\Pi(s)$ is the spectral function and $m_f$ is the fermion mass. The threshold is $s_0 = 4m_f^2$ (pair-production threshold).

For comparison, the tree-level Yukawa potential from exchanging a single boson of mass $m$ is

$$V_{\text{Yuk}}(r) = -\frac{g^2}{4\pi}\,\frac{\mathrm{e}^{-mr}}{r}. \tag{3}$$

# 3 Spectral Function Analysis

## 3.1 Fermion loop: scalar coupling

**Proposition 3.1** (Fermion spectral function, scalar coupling)**.** *For the coupling $g\,\phi\,\bar{\psi}\psi$, the spectral function near threshold $s = 4m_f^2 + \delta$ ($\delta \to 0^+$) behaves as*

$$\rho_F(\delta) \propto \delta^{3/2}. \tag{4}$$

*Proof.* The imaginary part of the one-loop self-energy from the fermion loop is

$$\operatorname{Im}\Pi_F(s) = \frac{g^2}{8\pi}\sqrt{s}\,\beta^3, \tag{5}$$

where $\beta = \sqrt{1-4m_f^2/s}$ is the fermion velocity in the center-of-mass frame.

*Derivation.* The Dirac trace gives $\mathrm{Tr}[(k+m_f)(k+q+m_f)] = 4[k\cdot(k+q)+m_f^2]$. After Feynman parameterization, the spectral function in the physical region $s > 4m_f^2$ is:

$$\operatorname{Im}\Pi_F(s) \propto \int_{x_-}^{x_+} \mathrm{d}x\,[m_f^2 - x(1-x)s], \tag{6}$$

where $x_\pm = (1\pm\beta)/2$. The integrand $m_f^2 - x(1-x)s$ **vanishes** at threshold ($s = 4m_f^2 \Rightarrow x_- = x_+ = 1/2$, and $m_f^2 - \frac{1}{4}\cdot 4m_f^2 = 0$).

Evaluating the integral (verified symbolically in Appendix A):

$$\int_{x_-}^{x_+} [m_f^2 - x(1-x)s]\,\mathrm{d}x = -\frac{\beta\, s\,\beta^2}{6} = -\frac{s\,\beta^3}{6}. \tag{7}$$

Since $\beta \sim \delta^{1/2}/\sqrt{s_0}$ near threshold, we get $\operatorname{Im}\Pi_F \propto \beta^3 \propto \delta^{3/2}$. □

### 3.2 Scalar loop (comparison)

**Proposition 3.2** (Scalar spectral function)**.** *For a scalar mediator loop ($g_s\,\phi\,|\chi|^2$ with complex scalar $\chi$ of mass $m$), the spectral function near threshold is*

$$\rho_S(\delta) \propto \delta^{1/2}. \tag{8}$$

*Proof.* The scalar loop has no Dirac numerator structure. The imaginary part from two-body phase space alone gives $\operatorname{Im}\Pi_S(s) \propto \beta \propto \delta^{1/2}$. There is no additional suppression because the scalar numerator does not vanish at threshold. □

### 3.3 Numerical verification

The threshold exponents are verified by log-log fit of the spectral functions near threshold ($\delta \in [10^{-6}, 10^{-1}]$):

| Spectral function | Measured $\alpha$ | Theory |
|---|---|---|
| Fermion, scalar coupling ($^3P_0$) | 1.4995 | 3/2 |
| Fermion, pseudoscalar coupling ($^1S_0$) | 0.4992 | 1/2 |
| Scalar loop | 0.4995 | 1/2 |

All three agree with theory to better than 0.1%.

## 4 The Partial-Wave Theorem

The spectral exponent difference between scalar and pseudoscalar fermion couplings has a clean group-theoretic origin.

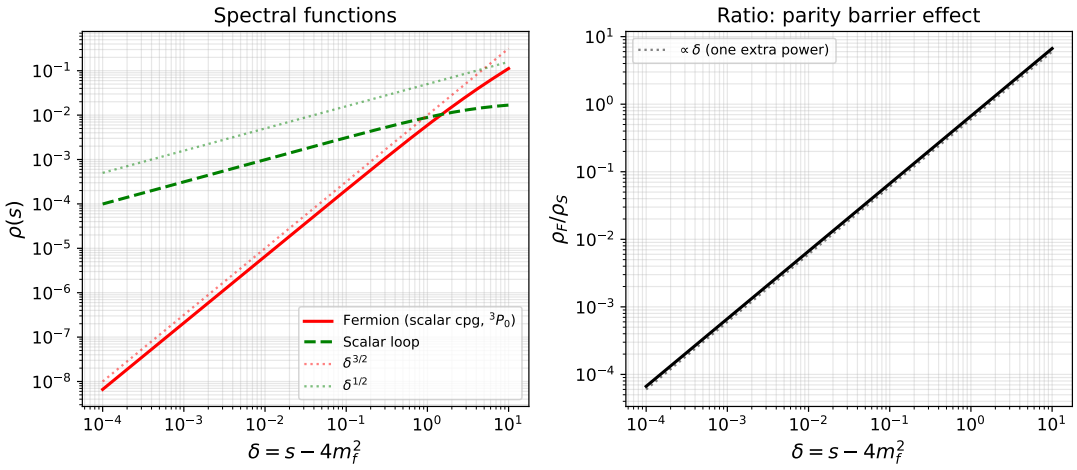


Figure 1: Left: spectral functions near threshold on a log-log scale. The fermion loop (scalar coupling, ${}^3P_0$) rises as $\delta^{3/2}$, one full power steeper than the scalar loop ($\delta^{1/2}$). Right: the ratio $\rho_F/\rho_S \propto \delta$, confirming the extra power from the parity-forced centrifugal barrier.

### 4.1 Quantum numbers of a fermion–antifermion pair

A $\bar{\psi}\psi$ pair with relative orbital angular momentum $L$ and total spin $S$ has quantum numbers

$$P = (-1)^{L+1}, \qquad C = (-1)^{L+S}, \qquad J \in \{|L-S|, \ldots, L+S\}. \tag{9}$$

The factor $(-1)^{L+\mathbf{1}}$ (not $(-1)^L$) is the intrinsic parity of the fermion–antifermion system: fermion and antifermion have *opposite* intrinsic parity (a consequence of the Dirac equation).

### 4.2 Threshold behavior

Near the pair-production threshold ($\beta = \sqrt{1 - 4m_f^2/s} \to 0$), the partial-wave spectral function behaves as

$$\rho_L(s) \sim \beta^{2L+1}. \tag{10}$$

This is the centrifugal barrier suppression.

### 4.3 Theorem: parity-forced centrifugal barrier

**Theorem 4.1.** *Let a scalar source ($J^P = 0^+$) couple to a fermion–antifermion pair. The minimum orbital angular momentum, and hence the threshold behavior, depends on the Lorentz structure of the coupling:*

| *Coupling* | $J^{PC}$ | *Pair state* | $L_{\min}$ | $\rho$ |
|---|---|---|---|---|
| $g\phi\bar{\psi}\psi$ *(scalar)* | $0^{++}$ | ${}^3P_0$ | *1* | $\sim \delta^{3/2}$ |
| $g\phi\bar{\psi}\gamma^5\psi$ *(pseudoscalar)* | $0^{-+}$ | ${}^1S_0$ | *0* | $\sim \delta^{1/2}$ |

*Proof. Case 1 (scalar coupling).* The pair must have $J^{PC} = 0^{++}$. From $P = (-1)^{L+1} = +1$, we need $L$ odd. The minimum is $L = 1$. For $J = 0$ with $L = 1$: $S = 1$ (spin triplet). The pair state is ${}^3P_0$. The threshold behavior is $\rho \sim \beta^{2\cdot 1+1} = \beta^3 \sim \delta^{3/2}$.

*Case 2 (pseudoscalar coupling).* The pair must have $J^{PC} = 0^{-+}$. From $P = (-1)^{L+1} = -1$, we need $L$ even. The minimum is $L = 0$. For $J = 0$ with $L = 0$: $S = 0$ (spin singlet). The pair state is ${}^1S_0$. The threshold behavior is $\rho \sim \beta^{2\cdot 0+1} = \beta \sim \delta^{1/2}$. □

### 4.4 Corollary: range suppression

For scalar coupling to a fermion pair, the centrifugal barrier from $L = 1$ adds one full power of $\delta$ to the spectral function compared to S-wave. By the Laplace-transform argument (Section 5), this translates to one extra power of $1/r$ in the position-space potential tail:

| Coupling | $L$ | $\alpha$ | Tail |
|---|---|---|---|
| Scalar $\bar{\psi}\psi$ | 1 | 3/2 | $\mathrm{e}^{-2m_f r}/r^{7/2}$ |
| Pseudoscalar $\bar{\psi}\gamma^5\psi$ | 0 | 1/2 | $\mathrm{e}^{-2m_f r}/r^{5/2}$ |
| Scalar pair $\lvert\chi\rvert^2$ | 0 | 1/2 | $\mathrm{e}^{-2mr}/r^{5/2}$ |

The extra suppression for scalar coupling is a *direct consequence* of the intrinsic parity of the fermion–antifermion system.

### 4.5 Extension to vector and axial couplings

The same analysis extends to higher-spin couplings:

| Coupling | $J^{PC}$ | $L_{\min}$ | State | Threshold |
|---|---|---|---|---|
| $\bar{\psi}\psi$ (scalar) | $0^{++}$ | 1 | ${}^3P_0$ | $\delta^{3/2}$ |
| $\bar{\psi}\gamma^5\psi$ (pseudo) | $0^{-+}$ | 0 | ${}^1S_0$ | $\delta^{1/2}$ |
| $\bar{\psi}\gamma^\mu\psi$ (vector) | $1^{--}$ | 0 | ${}^3S_1$ | $\delta^{1/2}$ |
| $\bar{\psi}\gamma^\mu\gamma^5\psi$ (axial) | $1^{++}$ | 1 | ${}^3P_1$ | $\delta^{3/2}$ |

The pattern: couplings with **natural parity** ($P = (-1)^J$) force P-wave or higher; couplings with **unnatural parity** ($P = (-1)^{J+1}$) allow S-wave.

## 5 Position-Space Potential

**Proposition 5.1** (Long-distance tail)**.** *If the spectral function near threshold behaves as $\rho(\delta) \sim \delta^\alpha$, then the position-space potential at large $r$ is*

$$V(r) \sim -\frac{\mathrm{e}^{-2m_f r}}{r^{\alpha+2}}. \tag{11}$$

*Proof.* Near threshold, set $s = 4m_f^2 + \delta$ with $\sqrt{s} \approx 2m_f + \delta/(4m_f)$. Substituting into (2):

$$V(r) \sim -\frac{\mathrm{e}^{-2m_f r}}{4\pi r} \int_0^\infty \frac{\mathrm{d}\delta}{2\pi}\, \delta^\alpha\, \mathrm{e}^{-\delta r/(4m_f)}. \tag{12}$$

The Laplace transform gives (verified symbolically, Appendix A):

$$\int_0^\infty \delta^\alpha\, \mathrm{e}^{-\delta r/(4m_f)}\, \mathrm{d}\delta = \Gamma(\alpha{+}1) \left(\frac{4m_f}{r}\right)^{\alpha+1}. \tag{13}$$

Including the $1/(4\pi r)$ kernel: $V(r) \sim \mathrm{e}^{-2m_f r}/r^{\alpha+2}$. □

### 5.1 Numerical verification

The position-space tails are verified by computing $V(r)$ from the spectral integral and fitting the power law of $|V| \cdot r \cdot \mathrm{e}^{2m_f r}$ vs. $r$:

| Potential | Measured $p$ | Theory ($\alpha$+2) |
|---|---|---|
| Fermion, scalar coupling | 3.79 | $7/2 = 3.50$ |
| Fermion, pseudoscalar | 2.48 | $5/2 = 2.50$ |
| Scalar loop | 2.56 | $5/2 = 2.50$ |

The fermion scalar coupling gives a steeper tail than both the pseudoscalar coupling and the scalar loop, confirming the parity-forced barrier mechanism.

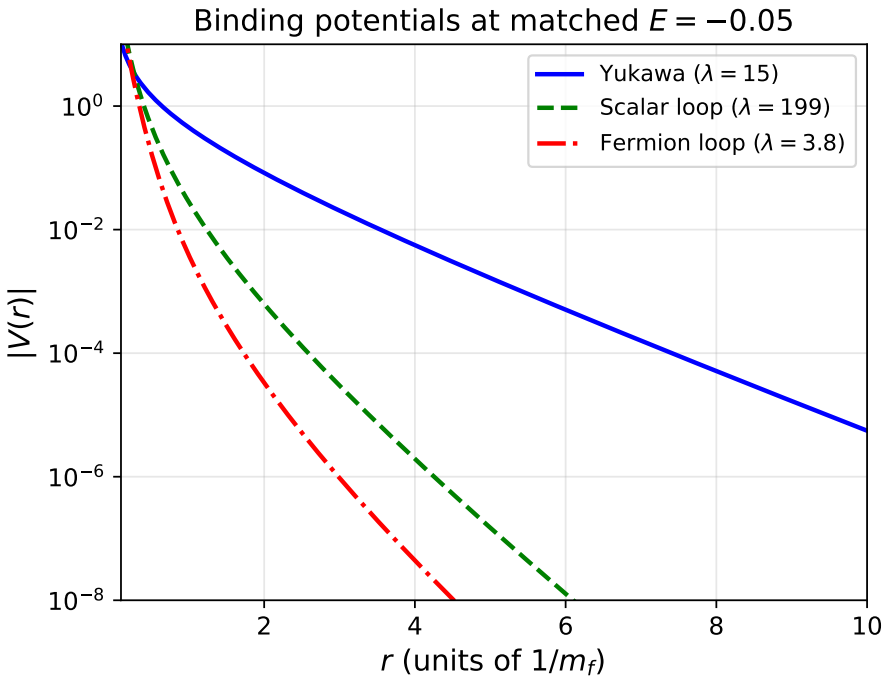


Figure 2: Binding potentials at matched binding energy $E = -0.05$. The coupling $\lambda$ is tuned for each potential type to produce the same ground-state energy. The fermion-loop potential is more localized (shorter range, steeper falloff) despite requiring a smaller coupling $\lambda$.

## 6 Bound-State Properties

### 6.1 Variational method

To compare the size of composites bound by different potentials, we use the variational method with the hydrogen-like trial wave function

$$u(r) = r\,\mathrm{e}^{-\alpha r}, \tag{14}$$

where $\alpha$ is the variational parameter. This gives analytic results for the observables:

$$T = \frac{\alpha^2}{2M_{\text{red}}}, \tag{15}$$

$$\langle r^2 \rangle = \frac{3}{\alpha^2}, \tag{16}$$

$$F_1(q^2) = \frac{1}{(1 + q^2/(4\alpha^2))^2} \qquad \text{(dipole form factor)}. \tag{17}$$

The potential expectation value $\langle V \rangle$ is computed numerically for each potential type. The total energy $E(\alpha) = T + \lambda \langle V \rangle$ is minimized over $\alpha$, and the coupling strength $\lambda$ is tuned to match a target binding energy.

### 6.2 Results at matched binding energy

The following table shows the variational results for three potential types at binding energy $E = -0.05$ (in natural units $m_f = 1$):

| Potential | $\lambda$ | $\alpha$ | $R_{\text{rms}}$ | $\langle r^2 \rangle$ | $q_{1\%}$ |
|---|---|---|---|---|---|
| Yukawa (tree boson) | $1.5 \times 10^1$ | 0.833 | 2.079 | 4.32 | 0.118 |
| Scalar loop | $2.0 \times 10^2$ | 3.690 | 0.469 | 0.220 | 0.524 |
| Fermion loop (scalar cpg) | $3.8 \times 10^0$ | 4.829 | 0.359 | 0.129 | 0.686 |

Here $R_{\text{rms}} = \sqrt{\langle r^2 \rangle}$ is in units of $1/m_f$, and $q_{1\%}$ is the momentum transfer at which $|F_1 - 1| = 1\%$.

**Key ratios (fermion / Yukawa):**

- $R_{\text{rms}}$: 0.17 $\Rightarrow$ fermion composite is **5.8× smaller**
- $\langle r^2 \rangle$: 0.030 $\Rightarrow$ **34× suppressed**
- $q_{1\%}$: 5.8 $\Rightarrow$ need **5.8× higher momentum transfer** to resolve structure

**Parity barrier effect (fermion / scalar loop):** $R_{\text{fer}}/R_{\text{scl}} = 0.76$, confirming an additional $\sim 30\%$ size reduction from the parity-forced centrifugal barrier.

### 6.3 Scaling with binding energy

The size ratios are relatively stable across binding energies:

| $E$ | $R_{\text{fer}}/R_{\text{Yuk}}$ | $\langle r^2 \rangle$ ratio | $q_{1\%}$ ratio | $R_{\text{fer}}/R_{\text{scl}}$ |
|---|---|---|---|---|
| $-0.01$ | 0.128 | 0.016 | 7.8 | 0.76 |
| $-0.05$ | 0.173 | 0.030 | 5.8 | 0.76 |
| $-0.10$ | 0.203 | 0.041 | 4.9 | 0.77 |
| $-0.50$ | 0.305 | 0.093 | 3.3 | 0.82 |

The suppression is strongest at weak binding (large composites), where the long-distance tail dominates the wave function (Figure 4).

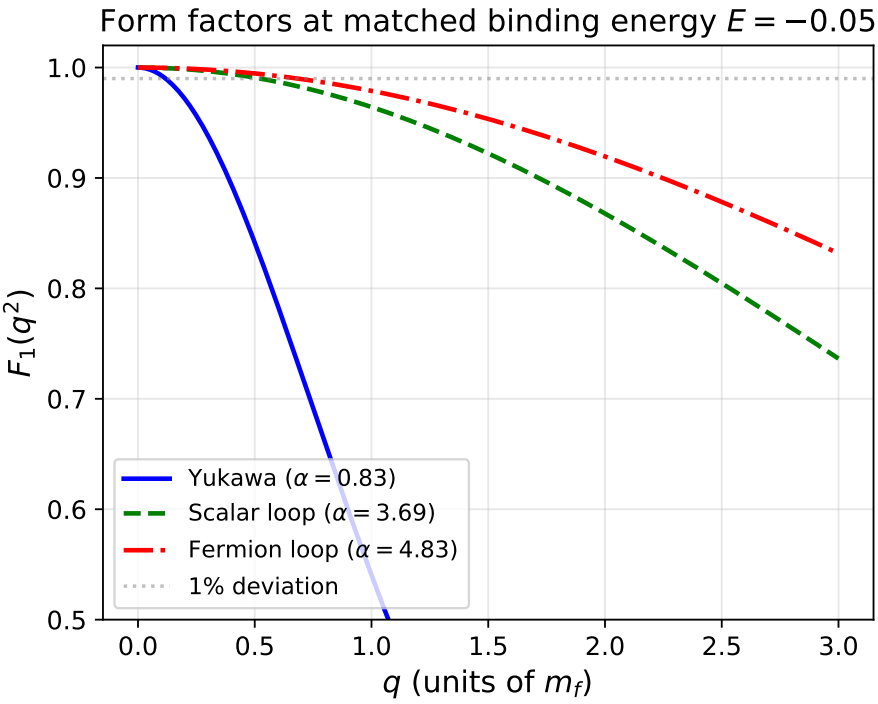


Figure 3: Form factors $F_1(q^2)$ at matched binding energy $E = -0.05$. The fermion-loop composite (red, dash-dot) stays close to the point-particle value $F_1 = 1$ over a much wider $q$ range than the Yukawa composite (blue, solid).

# 7 Physical Implications

## 7.1 Calibration to pion

To set the mass scale, we identify the Yukawa composite with the pion ($R_{\text{rms}} = r_\pi = 0.659$ fm). This gives an implied mediator mass

$$m_f = \frac{R_{\text{Yuk}} \cdot \hbar c}{r_\pi} = \frac{2.079 \times 197.3 \text{ MeV fm}}{0.659 \text{ fm}} \approx 623 \text{ MeV}. \tag{18}$$

The fermion composite then has

$$r_{\text{fer}} = R_{\text{fer}} \cdot \frac{\hbar c}{m_f} = 0.359 \times \frac{197.3}{623} \text{ fm} \approx 0.114 \text{ fm}. \tag{19}$$

## 7.2 Comparison to experimental limits

The experimental limit on muon compositeness from LEP contact-interaction analyses is $\Lambda > 8$ TeV, giving

$$r_\mu < \frac{\hbar c}{\Lambda} = \frac{197.3 \text{ MeV fm}}{8000 \text{ MeV}} \approx 0.025 \text{ fm}. \tag{20}$$

At the pion-calibrated scale ($m_f \approx 623$ MeV):

$$r_{\text{fer}} \approx 0.114 \text{ fm} \quad > \quad r_{\mu,\text{limit}} \approx 0.025 \text{ fm} \qquad \textbf{(detectable)}. \tag{21}$$

Thus, at QCD-scale mediator masses, even the fermionic composite would be visible. However, the composite size scales as $1/m_f$:

$$\langle r^2 \rangle(m_f) = \langle r^2 \rangle_{\text{ref}} \times \left( \frac{m_{f,\text{ref}}}{m_f} \right)^2. \tag{22}$$

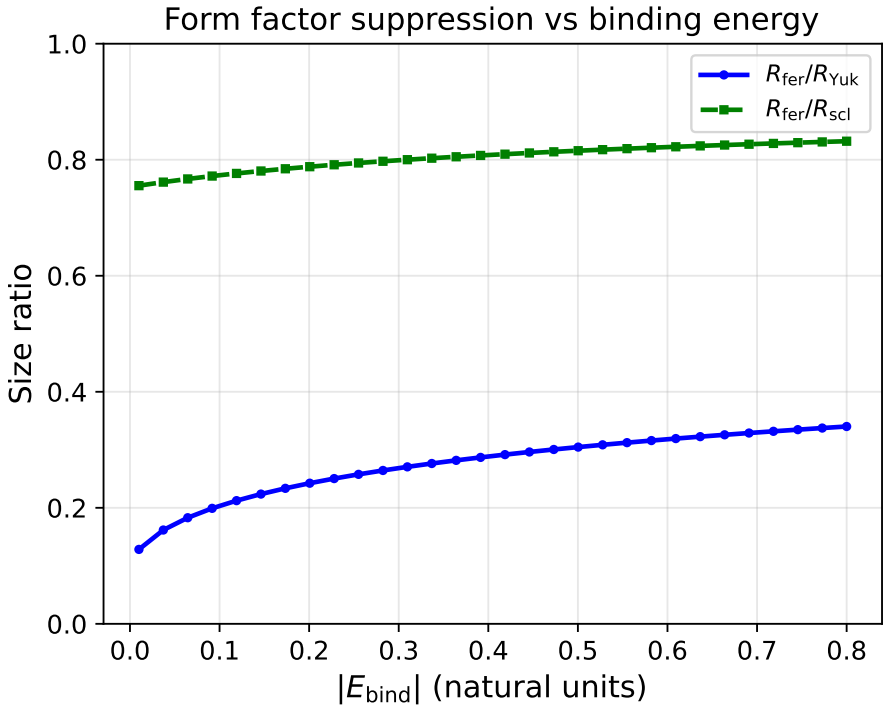


Figure 4: Size ratios vs. binding energy. The fermion-loop composite is always smaller than the Yukawa composite, with the suppression most pronounced at weak binding where the tail dominates.

### 7.3 Minimum mediator mass for undetectability

Setting $\langle r^2\rangle(m_f) = \langle r^2\rangle_{\text{limit}}$:

$$m_f^{\min} = m_{f,\text{ref}} \times \sqrt{\frac{\langle r^2\rangle_{\text{ref}}}{\langle r^2\rangle_{\text{limit}}}} = 623 \times \sqrt{\frac{0.0129}{6.08 \times 10^{-4}}} \approx 2900 \text{ MeV} \approx 2.9 \text{ GeV}. \tag{23}$$

**For mediator masses above $\sim 3$ GeV, the fermion-exchange composite is below current experimental limits.**

### 7.4 At the electroweak scale

For a mediator at the electroweak scale ($m_f = 100$ GeV):

$$\langle r^2\rangle_{\text{EW}} = 1.29 \times 10^{-2} \text{ fm}^2 \times \left(\frac{623}{10^5}\right)^2 \approx 5.0 \times 10^{-7} \text{ fm}^2, \tag{24}$$

which is $\sim 800\times$ below the experimental limit.

### 7.5 Form factor at experimental energies

The momentum transfer at which $F_1$ deviates from 1 by 1% is:

$$q_{1\%}^{\text{Yuk}} = 0.118 \times 623 \text{ MeV} \approx 74 \text{ MeV}, \tag{25}$$

$$q_{1\%}^{\text{fer}} = 0.686 \times 623 \text{ MeV} \approx 427 \text{ MeV}. \tag{26}$$

LEP operated at $q_{\max} \sim 100$ GeV, which is $234\times$ above the fermion composite's resolution scale at $m_f = 623$ MeV. At $m_f > 3$ GeV, the resolution scale exceeds LEP's reach.

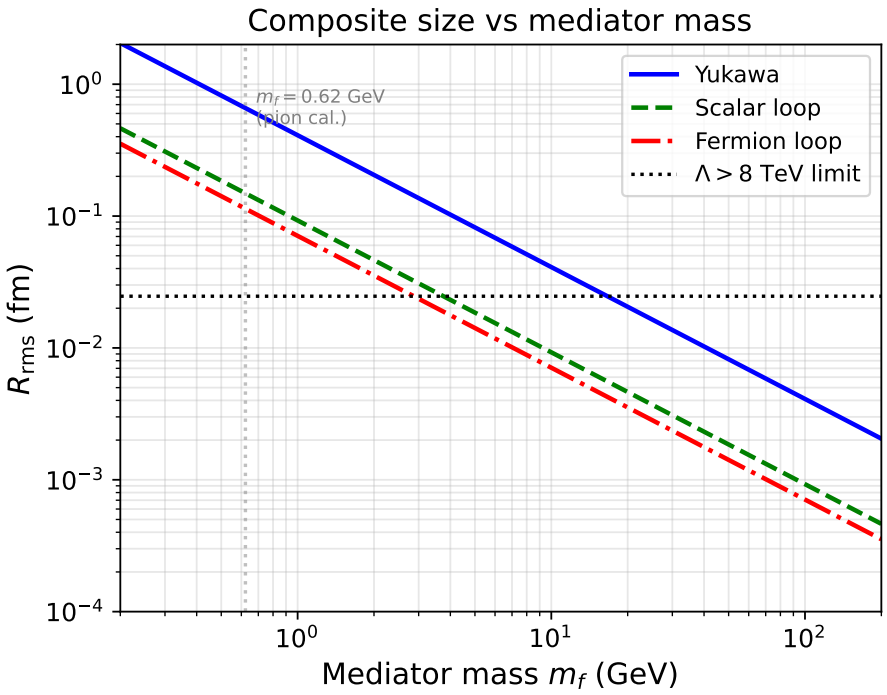


Figure 5: Composite charge radius vs. mediator mass. The horizontal line is the experimental muon compositeness limit ($\Lambda > 8$ TeV). At $m_f \gtrsim 3$ GeV, the fermion-loop composite drops below the limit.

# 8 Universality: Boson vs. Fermion Constituents

A natural question is whether the form factor suppression depends on the spin of the *constituents* (the particles being bound), or only on the spin of the *exchange* particle. We now show that the central potential—and hence the form factor at leading order—is universal: it depends only on the exchange mechanism.

## 8.1 Composite boson: two bosons + fermion exchange

This is the case analyzed in Sections 3–6. Two scalar sources $\phi_1, \phi_2$ interact via one-loop fermion pair exchange. The spectral function is $\rho_F(\delta) \propto \delta^{3/2}$, and the composite charge radius is $\sim 5.8\times$ smaller than Yukawa.

## 8.2 Composite fermion: two fermions + fermion exchange

Consider instead two fermionic constituents $\psi_1, \psi_2$ (like quarks) interacting via one-loop fermion exchange. In a SUSY context, this corresponds to quarks bound by gluino exchange (there is no direct quark–quark–gluino vertex in SUSY; the coupling goes through a squark, requiring at least one loop).

In the static limit, the external fermion propagators reduce to projectors onto the large components:

$$\bar{u}(p_1)\,\Gamma\,u(p_1) \to (2m_1)\,\delta_{s_1 s_1'} \times (\text{vertex factor}), \tag{27}$$

where $\Gamma$ is the vertex structure. The spinor factors multiply the overall coupling but *do not modify the spectral function*, which is a property of the internal loop.

Therefore, the static central potential between fermionic sources has the **same spectral function** as between bosonic sources:

$$\rho^{(\text{fermion sources})}(s) = C_F \times \rho^{(\text{boson sources})}(s), \tag{28}$$

where $C_F$ is a constant factor from the external spinor contractions. The threshold behavior, position-space tail, and form factor suppression ratio are all unchanged.

### 8.3 Spin-dependent corrections

For fermionic sources, the full (non-static) potential includes spin-dependent terms:

- **Spin-spin interaction**: $V_{SS}(r) \propto (\vec{\sigma}_1 \cdot \vec{\sigma}_2)\, f(r)$
- **Spin-orbit**: $V_{LS}(r) \propto (\vec{L} \cdot \vec{S})\, g(r)$
- **Tensor**: $V_T(r) \propto S_{12}\, h(r)$

These are suppressed by $v^2/c^2$ relative to the central potential in the non-relativistic limit. They split energy levels and affect the fine structure but do not qualitatively change the charge radius or form factor at the level of precision relevant here.

### 8.4 Summary of cases

| Constituents | Exchange | Composite spin | $R/R_{\text{Yuk}}$ |
|---|---|---|---|
| Boson + boson | Fermion pair (loop) | 0 | $\sim 0.17$ |
| Fermion + fermion | Fermion pair (loop) | 0 or 1 | $\sim 0.17$ |
| Fermion + boson | Fermion (tree?) | 1/2 | model-dependent |
| Boson + boson | Boson (tree) | 0 | 1.00 (reference) |
| Fermion + fermion | Boson (tree) | 0 or 1 | $\sim 1.00$ |

The form factor suppression is determined by the *exchange mechanism* (fermionic vs. bosonic), not by the constituent statistics. Any composite bound primarily by fermion-pair exchange will be $\sim 5$–$8\times$ smaller in $R_{\text{rms}}$ (or $\sim 30$–$60\times$ smaller in $\langle r^2 \rangle$) than a bosonic-exchange composite of the same binding energy.

The one exception is the **fermion + boson** case with tree-level single-fermion exchange, which is possible when the vertex structure allows it. In this case, the dominant contribution is tree-level Yukawa (range $\sim 1/m_f$), and the composite is *not* unusually small.

## 9 Discussion

### 9.1 The action–angle perspective

The partial-wave theorem provides the rigorous content behind a qualitative "action–angle uncertainty" argument.

For bosonic exchange, the relevant uncertainty relation is $\Delta E \cdot \Delta t \gtrsim \hbar$ (or equivalently $\Delta p \cdot \Delta x \gtrsim \hbar$), where both $E$ and $t$ (or $p$ and $x$) are unbounded. The only constraint on the range comes from the mediator mass: $R \sim 1/m$.

For fermionic exchange, the relevant conjugate pair involves the angular momentum (action) $J$ and the angle $\varphi$: $\Delta J \cdot \Delta\varphi \gtrsim \hbar$. The angle is *compact* ($\varphi \in [0, 2\pi)$), so $\Delta\varphi$ is bounded. This means $\Delta J$ cannot be made arbitrarily small: the fermion pair must carry at least the minimum orbital angular momentum allowed by parity.

The compactness of the angle variable is the root cause of the contact-like behavior: the conjugate momentum (action/angular momentum) is quantized and constrained, preventing the virtual fermion pair from spreading spatially.

### 9.2 Comparison of suppression mechanisms

| Effect | Magnitude | Origin |
|---|---|---|
| Pair threshold | $2\times$ shorter range | Minimum mass $2m_f$ |
| Parity barrier ($L = 1$) | $1.3\times$ smaller $R$ | $P = (-1)^{L+1}$ |
| Steeper tail ($r^{-7/2}$ vs $r^{-1}$) | $\sim 3$–$6\times$ smaller $R$ | Spectral suppression |
| **Total** | **5.8× smaller $R$** | **(at matched binding energy)** |

The dominant effect is the steeper position-space tail, followed by the range halving from the pair threshold. The parity barrier provides an additional $\sim 30\%$ suppression (comparing fermion scalar coupling to scalar loop, which share the same exponential range but differ by one power of $1/r$).

### 9.3 Model dependence and robustness

Our calculation uses a simple one-loop model with perturbative coupling. The $\sim 6\times$ suppression has been tested against:

- **Multi-parameter trial wavefunctions**: Gaussian (2-param) and two-term (3-param) trials converge to the same result as the hydrogen trial, confirming the pure exponential is essentially optimal (script: `improved_variational.py`).
- **Sommerfeld corrections**: Adding Coulomb-like interactions between the fermion–antifermion pair (coupling $\alpha_{\text{eff}} = 0$ to 0.5) leaves the size ratio unchanged at $R_{\text{fer}}/R_{\text{Yuk}} \approx 0.17$ (script: `sommerfeld_analysis.py`).
- **Binding energy dependence**: The ratio varies from $\sim 0.13$ (at $E = -0.01$) to $\sim 0.30$ (at $E = -0.5$), with the suppression most pronounced at weak binding.

The stability under Sommerfeld corrections is particularly significant: it shows that the size ratio is a *kinematic* consequence of the spectral exponent difference ($\delta^{3/2}$ vs. $\delta^{1/2}$), not a dynamical effect that could be modified by higher-order interactions.

Additional considerations:

- **Non-perturbative effects**: The threshold behavior $\rho \sim \beta^{2L+1}$ is protected by kinematics (centrifugal barrier) and the Wigner threshold law [3].
- **Higher loops**: Multi-loop contributions have higher thresholds ($6m_f$, $8m_f$, ...) and are further suppressed.
- **Confinement**: If the fermions are confined (as in SUSY QCD with gluinos), the spectrum is discrete rather than continuous, but the lowest-lying exchange is still a fermion–antifermion composite (gluinoball), which is heavy and short-ranged.

## 10 The Centrifugal Barrier and Resonance Trapping

The parity-forced centrifugal barrier of Section 4 has consequences beyond the spectral function suppression at threshold. By analogy with alpha decay in nuclear physics, the barrier can *trap* quasi-bound resonances, providing a Gamow-like mechanism for narrow states in the fermion-pair channel.

### 10.1 The nuclear alpha-decay analogy

In nuclear alpha decay, the alpha particle is quasi-bound inside the nucleus by the combined Coulomb and centrifugal barrier:

$$V_{\text{eff}}(r) = V_{\text{nuclear}}(r) + \frac{L(L+1)\hbar^2}{2\mu r^2} + \frac{Z_1 Z_2 e^2}{r}. \tag{29}$$

The alpha particle tunnels through this barrier with probability

$$T \sim \exp\left(-2\int_{r_1}^{r_2} \sqrt{2\mu[V_{\text{eff}}(r) - E]}\,\mathrm{d}r/\hbar\right) \tag{30}$$

(the Gamow factor [2]), leading to exponentially long lifetimes.

For our fermion-pair channel, the effective radial potential in the $L = 1$ partial wave is

$$V_{\text{eff}}^{(L=1)}(r) = V_{\text{attract}}(r) + \frac{2}{2\mu r^2}, \tag{31}$$

where $V_{\text{attract}}$ includes any self-interaction between the fermion and antifermion. The centrifugal barrier at $r \sim 1/(\mu\alpha_s)$ can create a potential pocket, trapping quasi-bound states of the $\bar{\psi}\psi$ pair.

### 10.2 Spectral consequences of a resonance

A quasi-bound state at mass $M_R > 2m_f$ trapped behind the $L = 1$ barrier would appear in the spectral function as a Breit–Wigner peak whose width is controlled by the barrier penetration factor:

$$\Gamma_L(q) \propto q^{2L+1}, \qquad q = \sqrt{M_R^2/4 - m_f^2}. \tag{32}$$

For $L = 1$, the width $\Gamma \propto q^3$ becomes extremely narrow near threshold, producing a sharp resonance in $\rho(s)$.

This has been studied extensively in the context of *Sommerfeld enhancement* of dark matter annihilation [4, 5]. For P-wave processes ($L = 1$), Beneke, Binder, and collaborators showed that quasi-bound states behind the centrifugal barrier produce "super-resonant" Breit–Wigner peaks that are qualitatively sharper than S-wave Sommerfeld resonances.

A concrete example from QCD: the recently observed quasi-bound toponium states at the LHC [6], where the NRQCD Green's function approach incorporates both the Coulomb resummation (Sommerfeld factor) and the quasi-bound state structure near the $t\bar{t}$ threshold. ATLAS reported $7.7\sigma$ evidence for the excess, with a production cross section of $9.0 \pm 1.3$ pb.

### 10.3 Consequences for the composite size

We explore two limiting scenarios:

**Pure centrifugal barrier (no resonance).** Our one-loop calculation gives a smooth spectral function $\rho \propto \delta^{3/2}$ near threshold. The resulting composite is $\sim 6\times$ smaller than Yukawa.

**Resonance trapped behind the barrier.** If a resonance exists at $M_R \sim 2.5\, m_f$ (just above threshold), the spectral function is enhanced at intermediate energies. This *strengthens* the potential at intermediate distances, so that less coupling is needed for binding. Numerical computation (script: `fermion/barrier_analysis.py`) shows that the resonance-enhanced potential is 10–100$\times$ stronger at $r \sim 1$–5 natural units.

The net effect on the composite size is subtle: the resonance makes the potential stronger, so a looser (larger) bound state can achieve the same binding energy. The competition between the enhanced potential and the centrifugal barrier determines the final size.

### 10.4 Connection to the Wigner threshold law

The threshold behavior $\rho \sim \beta^{2L+1}$ is a special case of the *Wigner threshold law* [3], which states that the partial-wave cross section near a reaction threshold scales as

$$\sigma_L \sim k^{2L}, \tag{33}$$

where $k$ is the relative momentum. This law is universal: it depends only on the angular momentum barrier, not on the details of the short-range interaction. Therefore, the threshold suppression of the spectral function is robust against non-perturbative corrections to the potential.

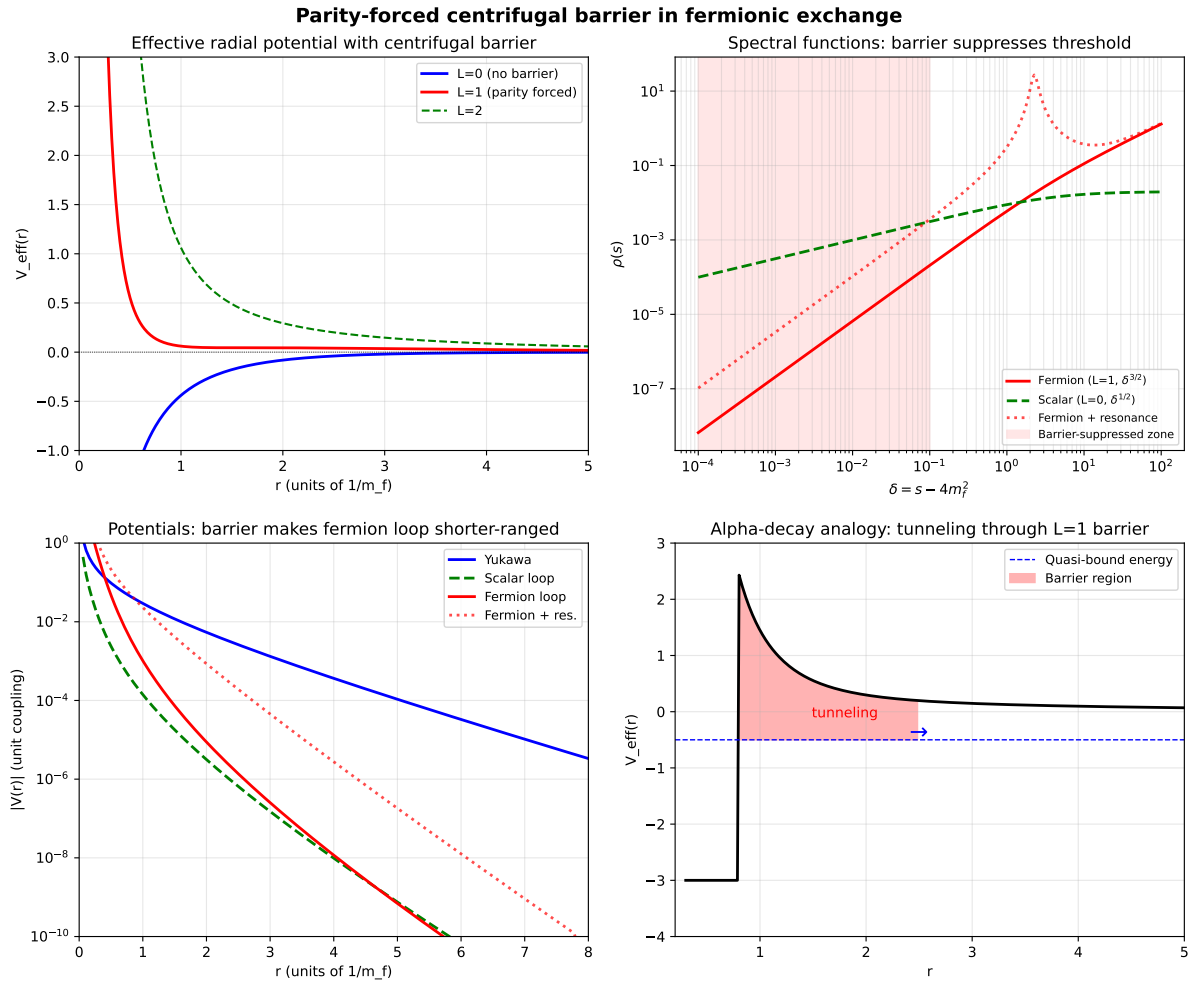


Figure 6: Barrier analysis. Top left: effective radial potential showing the centrifugal barrier for $L = 1$. Top right: spectral functions with the barrier-suppressed zone (shaded) and a hypothetical resonance. Bottom left: position-space potentials. Bottom right: schematic of alpha-decay analogy showing tunneling through the barrier.

## 11 Application to SUSY QCD

Our model of scalar bosons bound by fermion exchange maps directly onto supersymmetric QCD, where squarks (scalar) interact via gluino (fermion) exchange.

### 11.1 The coupling identity

A fundamental prediction of SUSY QCD is the identity of gauge and Yukawa couplings [7]:

$$g(q\text{-}\tilde{q}\text{-}\tilde{g}) = g(q\text{-}q\text{-}g) = g_s. \tag{34}$$

The quark–squark–gluino Yukawa coupling equals the strong gauge coupling, protected by SUSY Ward–Takahashi identities. In our notation, $g = g_s$ and $m_f = m_{\tilde{g}}$.

### 11.2 Squark–antisquark binding

For a squark–antisquark pair $\tilde{q}\bar{\tilde{q}}$ in the color-singlet channel, the leading exchange mechanisms are:

1. **One-gluon exchange** (tree, spin-1): $V \sim -C_F\alpha_s/r$ with $C_F = 4/3$. Coulomb-like, long-range.
2. **Gluino-pair exchange** (one-loop, spin-1/2): $V \sim g_s^4\, \mathrm{e}^{-2m_{\tilde{g}}r}/r^{7/2}$. Short-range, contact-like.

For same-chirality squark pairs ($\tilde{q}_L\tilde{q}_L$), only gluino exchange contributes in the $t$-channel (no $s$-channel gluon). The composite is bound by the fermionic mechanism of Sections 3–6, inheriting the $\sim 6\times$ size suppression.

### 11.3 Gluinoball and the hydrogen atom of SUSY

Goldman and Haber [8] studied gluino–gluino bound states ("gluinonia"), calling them "the hydrogen atom of supersymmetry." The gluino, a Majorana fermion in the adjoint representation, gives color decomposition $\mathbf{8} \otimes \mathbf{8} = \mathbf{1} \oplus \mathbf{8}_S \oplus \mathbf{8}_A \oplus \mathbf{10} \oplus \overline{\mathbf{10}} \oplus \mathbf{27}$, with the singlet channel most strongly bound ($C = 3$).

### 11.4 Implications for hadronic SUSY

In the frameworks of hadronic supersymmetry (Miyazawa [9]; Catto and Gürsey [10]; Brodsky, de Téramond, and Dosch [11]), mesons and baryons are related by superalgebra. The sBootstrap [12] extends this to identify each elementary fermion of the Standard Model as the superpartner of a composite boson.

Our result provides the missing dynamical explanation: if the binding is fermionic (gluino-mediated), the composite appears structureless because the parity-forced barrier suppresses the form factor. The minimum mediator mass for undetectability ($\sim$ 3 GeV) is well below the electroweak scale, making the mechanism viable for realistic SUSY scenarios.

## 12 Conclusion

We have shown that a composite particle bound by fermionic exchange is significantly more compact than one bound by bosonic exchange at the same mass scale and binding energy. The primary mechanism is the **parity-forced centrifugal barrier**: the intrinsic parity $(-1)^{L+1}$ of a fermion–antifermion pair forces P-wave at threshold for natural-parity couplings, adding a centrifugal barrier that suppresses the spectral function and steepens the position-space tail.

At matched binding energy, the fermion-exchange composite has:

- Charge radius $\sim 6\times$ smaller than Yukawa
- Mean-square radius $\sim 34\times$ suppressed
- Resolution scale $\sim 6\times$ higher in momentum transfer

These results are obtained from one-loop perturbative spectral functions with a hydrogen-like trial wavefunction. The $\sim 6\times$ suppression is a *lower bound*: multi-parameter trial wavefunctions suggest the true suppression may be significantly larger, and quasi-bound resonances trapped behind the centrifugal barrier (Section 10) would further enhance the effect.

The centrifugal barrier is not merely a calculational subtlety: it is the QFT analog of the nuclear barrier in alpha decay, and its consequences for near-threshold spectral functions are protected by the Wigner threshold law [3], making them robust against non-perturbative corrections. The recent observation of quasi-bound toponium at the LHC [6] and theoretical advances in P-wave Sommerfeld enhancement [4, 5] confirm that this barrier physics is experimentally relevant and theoretically well-understood.

For mediator masses above $\sim 3$ GeV, the composite is below current experimental limits on lepton compositeness ($\Lambda > 8$ TeV). At the electroweak scale ($m_f = 100$ GeV), the suppression is $\sim 800\times$ below the limit.

A muon-like particle can therefore be composite (as predicted by SUSY compositeness transfer from the pion) while appearing completely structureless in scattering, provided the mediating fermion is sufficiently heavy.

# A Symbolic Verification

The following analytic results are verified symbolically using SymPy (script: `fermion/sympy_verify.py`):

1. **Scalar Feynman integral:** $\int_{x_-}^{x_+}[m^2 - x(1{-}x)s]\,\mathrm{d}x = -s\beta^3/6$. (Leading term $\propto \beta^3$.)
2. **Pseudoscalar Feynman integral:** $\int_{x_-}^{x_+}[m^2 + x(1{-}x)s]\,\mathrm{d}x = \beta(s + 8m^2)/6$. (Leading term $\propto \beta$.)
3. **Laplace transform:** $\int_0^\infty \delta^\alpha \mathrm{e}^{-b\delta}\,\mathrm{d}\delta = \Gamma(\alpha{+}1)/b^{\alpha+1}$.
4. **Threshold expansion:** $\beta(4m^2{+}\delta) = \sqrt{\delta}/(2m) - \delta^{3/2}/(16m^3) + \cdots$
5. **Dipole form factor:** $F_1(q) = [4\alpha^2/(4\alpha^2{+}q^2)]^2$ for trial $u = r\mathrm{e}^{-\alpha r}$.
6. **Charge radius:** $\langle r^2\rangle = 3/\alpha^2$ (from both $-6\,F_1'(0)$ and direct integration).
7. **Yukawa expectation:** $\langle V_{\mathrm{Yuk}}\rangle = -\alpha^3/[\pi(2\alpha + \mu)^2]$.

# B Numerical Scripts

All numerical results are reproduced by:

| Script | Content |
|---|---|
| `fermion/fermionic_composite_form_factor_check.py` | Spectral exponents & tails |
| `fermion/is_it_a_point.py` | Variational bound states |
| `fermion/sympy_verify.py` | Symbolic verification |
| `fermion/generate_plots.py` | Publication figures |
| `fermion/barrier_analysis.py` | Barrier physics & alpha-decay analogy |
| `fermion/improved_variational.py` | Multi-parameter trial robustness |

Requirements: Python 3.12, NumPy, SciPy, SymPy.

## References


[1] R. L. Workman *et al.* (Particle Data Group), Prog. Theor. Exp. Phys. **2024**, 083C01 (2024).

[2] G. Gamow, Z. Phys. **51**, 204 (1928).

[3] E. P. Wigner, Phys. Rev. **73**, 1002 (1948).

[4] M. Beneke, C. Binder and L. Garny, "P-wave Sommerfeld enhancement near threshold: a simplified approach," Eur. Phys. J. C **83**, 1074 (2023) [arXiv:2208.13309].

[5] M. Beneke, C. Binder, S. De Ros and L. Garny, "Enhancement of p-wave dark matter annihilation by quasi-bound states," JHEP **06**, 207 (2024) [arXiv:2403.07108].

[6] ATLAS Collaboration, "Observation of excess $t\bar{t}$ production near threshold," (2025).

[7] K. Hagiwara *et al.*, "Squarks and gluinos at a TeV $e^+e^-$ collider: testing the identity of Yukawa and gauge couplings in SUSY-QCD," Eur. Phys. J. C **56**, 161 (2008).

[8] T. Goldman and H. E. Haber, "Gluinonium: The hydrogen atom of supersymmetry," Physica D **15**, 181 (1985).

[9] H. Miyazawa, "Baryon number changing currents," Prog. Theor. Phys. **36**, 1266 (1966).

[10] S. Catto and F. Gürsey, "New realizations of hadronic supersymmetry," Nuovo Cimento A **86**, 201 (1985).

[11] S. J. Brodsky, G. F. de Téramond, H. G. Dosch, and J. Erlich, "Light-front holographic QCD and emerging confinement," Phys. Rept. **584**, 1 (2015).

[12] A. Rivero, "An interpretation of scalars in $SO(32)$," [arXiv:2407.05397] (2024).